ADVANCED FUNCTIONAL MATERIALS
www.afm-journal.de

www.MaterialsViews.com

Massive Anisotropic Thermal Expansion and Thermo-Responsive Breathing in Metal–Organic Frameworks Modulated by Linker Functionalization

Sebastian Henke, Andreas Schneemann, and Roland A. Fischer**

Functionalized metal–organic frameworks (fu-MOFs) of general formula $[Zn_2(fu\text{-}L)_2dabco]_n$ show unprecedentedly large uniaxial positive and negative thermal expansion (fu-L = alkoxy functionalized 1,4-benzenedicarboxylate, dabco = 1,4-diazabicyclo[2.2.2]octane). The magnitude of the volumetric thermal expansion is more comparable to property of liquid water rather than any crystalline solid-state material. The alkoxy side chains of fu-L are connected to the framework skeleton but nevertheless exhibit large conformational flexibility. Thermally induced motion of these side chains induces extremely large anisotropic framework expansion and eventually triggers reversible solid state phase transitions to drastically expanded structures. The thermo-responsive properties of these hybrid solid–liquid materials are precisely controlled by the choice and combination of fu-Ls and depend on functional moieties and chain lengths. In principle, this combinatorial approach allows for a targeted design of extreme thermo-mechanical properties of MOFs addressing the regime between crystalline solid matter and the liquid state.

1. Introduction

Inorganic-organic hybrid materials receive much attention,[1] and among those metal–organic frameworks (MOFs) are particularly interesting for academic research and much promising for industrial applications.[2] MOFs are robust, porous and crystalline materials, which are based on Werner-type coordination chemistry and are constructed from metal ions, which are interconnected by organic linkers, L (i.e., multitopic carboxylates, imidazolates, etc.), in two or three dimensions in space. The resulting zeolite-like architectures define the coordination space of guest accessible pores and channels. Huge topological diversity paired with extraordinary chemical versatility and designability suggest diverse applications, including gas storage,[3] separation,[4] catalysis,[5] etc. A straightforward way to fine tune MOFs is attaching additional functional groups (**fu** s) at the linker L. This concept is not at all restricted to trivial choices of substituents (**fu** = NH_2, NO_2, OH, etc.),[6] but can be expanded to more sophisticated **fu**s like alkyl amides[7] or even crown ethers and rotaxanes.[8] Typically, **fu**s are not as ordered as the crystalline scaffold, rather they point more or less randomly into the cavities and exhibit a certain degree of conformational flexibility.[8,9] Often the respective fu-MOFs exhibit an increased structural complexity based on the coalescence of the highly regular framework skeletons and the disordered **fu**s in void space.

Recently, we have shown that implementation of additional alkoxy groups at bdc-type linkers (bdc = 1,4-benzenedicarboxylate) can initiate unexpected guest-dependent structural flexibility in so-called pillared-layered MOFs of the general formula $[Zn_2(fu\text{-}L)_2dabco]_n$ (**Figure 1**; fu-L = alkoxy functionalized bdc, dabco = 1,4-diazabicyclo[2.2.2]octane).[10] The responsive networks are constructed from binuclear Zn_2-paddlewheel units, which are 2D-interconnected by fu-L and bridged in the third dimension by dabco as pillar (Figure 1b,c). In contrast to the non-functionalized parent framework $[Zn_2bdc_2dabco]_n$,[11] the corresponding functionalized derivatives $[Zn_2(fu\text{-}L)_2dabco]_n$ reversibly switch between an extended large pore (*lp*) and a drastically contracted narrow pore (*np*) form as a function of guests adsorption (Figure 1d). Reasons for the guest-dependent bistability are attractive dipolar and dispersion interactions between adjacent **fu**, between guests and **fu**, as well as between **fu** and the framework backbone.[10a,10c]

Such kind of flexible or adaptive MOFs, also named soft porous crystals,[12] have been studied intensively in terms of their unique 'breathing' or 'gate opening' phenomena upon guest adsorption, which are very attractive for smart separation[4] and sensing applications.[13] Reports on the *intrinsic* softness of MOFs in *absence* of any guests are very rare, however.[14] Anomalous thermo-mechanical properties, like 'colossal' positive thermal expansion[15] (PTE) as well as uniaxial or volumetric negative thermal expansion[16] (NTE) have been reported only recently. These studies have merely focused on

Dr. S. Henke
Department of Materials Science and Metallurgy
University of Cambridge
Pembroke Street, Cambridge CB2 3QZ, UK
E-mail: sh738@cam.ac.uk
Dr. S. Henke, A. Schneemann, Prof. R. A. Fischer
Lehrstuhl für Anorganische Chemie II
Ruhr-Universität Bochum
Universitätsstraße 150, 44780 Bochum, Germany
E-mail: roland.fischer@rub.de

DOI: 10.1002/adfm.201301256

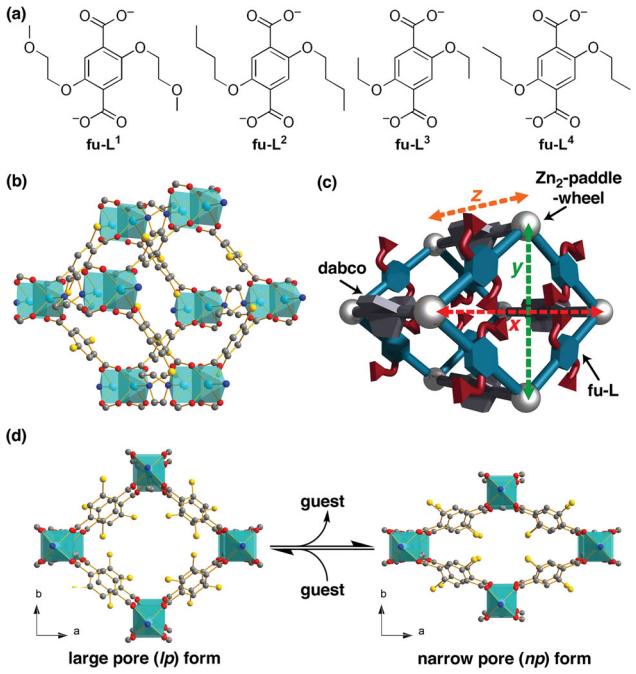

Figure 1. a) Selection of alkoxy functionalized 1,4-benzenedicarboxylates (fu-Ls) used in this work. b) Cut-out of the structure of as-prepared $[Zn_2(fu\text{-}L^1)_2dabco]_n$ (**1**).[10a] Disordered moieties of fu-L^1 and dabco have been omitted for clarity. The flexible side chains are not included in the structural model. H atoms are not shown. c) Structural representation depicting the lattice vectors *x*, *y*, and *z*. d) Representation of the reversible *lp*→*np* transition of **1** upon guest molecule removal/re-adsorption at ambient temperature. Colour code for b and d: Zn polygons (cyan), O (red), N (blue), C (grey); yellow spheres indicate the positions of **fu**.

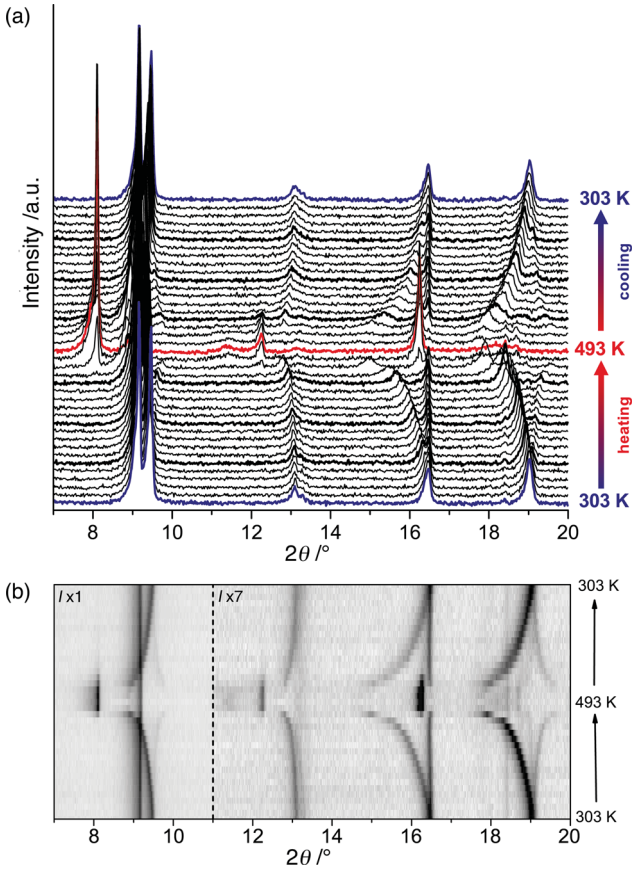

Figure 2. VT-PXRD patterns of $[Zn_2(fu\text{-}L^1)_2dabco]_n$ (**1**) recorded from 303 to 493 K (ΔT/step = 10 K). a) Conventional representation, b) representation as an artificial 2D film.

dense coordination networks without guest accessible voids. A rational strategy for the implementation and modulation of such 'extreme' thermo-mechanical properties in *porous* coordination networks, i.e. prototypical MOFs, is absent, so far.

Here we show, that the unique interplay of a structurally well-defined framework backbone decorated with disordered, conformationally flexible substituents results in extraordinary thermo-mechanical responsiveness. Variable temperature powder X-ray diffraction (VT-PXRD) and differential scanning calorimetry (DSC) measurements of a variety of guest-free $[Zn_2(fu\text{-}L^k)_2dabco]_n$ (k = 1–4, Figure 1a) frameworks reveal massive PTE, uniaxial NTE, as well as adjustable thermo-responsive breathing (reversible *np*→*lp* transition *without* guest adsorption) associated to the intrinsic nature of these hybrid solid/liquid materials.

2. Results and Discussion

VT-PXRD patterns of the prototypic, guest-free framework $[Zn_2(fu\text{-}L^1)_2dabco]_n$ (**1**), which features pendent 2-methoxyethoxy substituents, were recorded in the temperature range from 303 to 493 K with a step size of 10 K (**Figure 2**). The diffraction patterns give evidence for drastic but fully reversible structural changes of **1** depending on the temperature. Le Bail fitting analysis[17] of the VT-PXRD patterns was performed to quantify the temperature-driven structural changes (unit cell parameters, space group symmetry). In order to allow for an easy description we define the characteristic lattice vectors *x*, *y*, and *z* (Figure 1c), which are independent from the respective crystal symmetry of the *np* and *lp* phases (monoclinic vs. tetragonal, Supporting Information Figure S50). Vectors *x* and *y* represent the diagonals characteristic for the 2D $[Zn_2(fu\text{-}L)_2]_n$ grid and *z* represents the repeat distance of two neighboring $[Zn_2(fu\text{-}L)_2]_n$ grids along the dabco axis. The specific volume (V_{spec}) is defined as the crystallographic volume per formula unit. **Figure 3** displays the temperature dependent structural changes of **1** on the basis of *x*, *y*, *z*, and V_{spec}. Three facts are immediately apparent from the data. Firstly, **1** exists solely in the contracted *np* form at 303 K and shows massive thermal expansion in the range from 303 to 463 K, leading to a 4.5% increase in V_{spec} over a range of just 160 K. Secondly, between 473 to 493 K, **1** transforms from the *np* to the *lp* form involving a 19% increase in V_{spec} with respect to the *np* form at 303 K. And, thirdly, the thermal expansion as well as the phase transition is completely reversible. Similar to the thermal breathing of MIL-53(Al), **1** features a hysteretic behavior leading to a shift of the reverse *lp*→*np* transition to lower temperatures (473 to 453 K) on the cooling branch of the VT-PXRD experiment. However, the width of the hysteresis is very narrow (≈20 K)

ADVANCED FUNCTIONAL MATERIALS
www.afm-journal.de

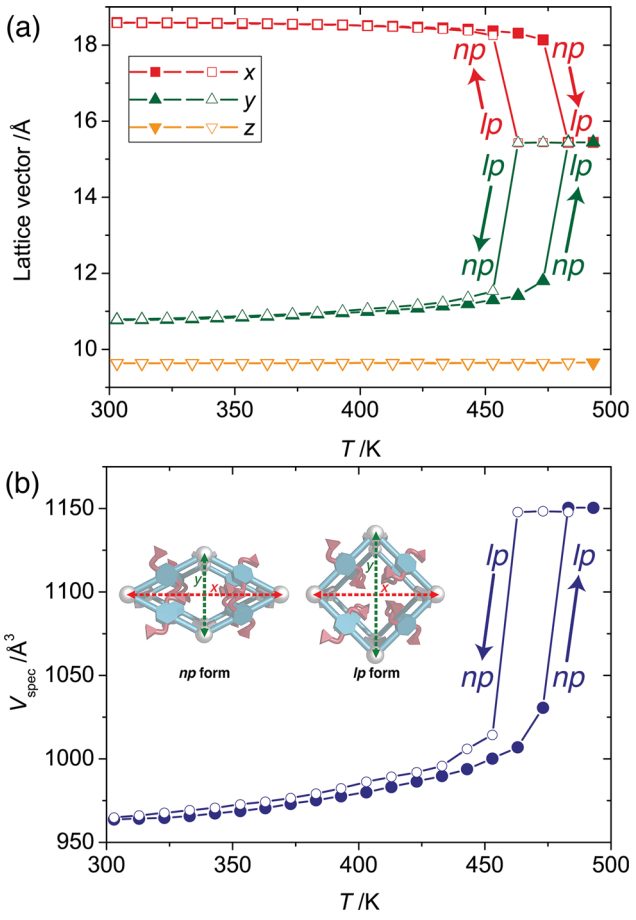

Figure 3. a) Evolution of lattice vectors *x*, *y*, *z* and b) specific volume V_{spec} of **1** in dependence on the temperature. Data points of the heating and cooling branches are shown as solid and open symbols, respectively. The errors are not larger than the size of the symbols. Note that in the range from 473 to 483 K on the heating branch and 473 to 453 K on the cooling branch both phases (*np* and *lp*) coexist in varying ratios. Only the majority phase at these temperatures is included in the graphs. The insert in panel b shows a graphical representation of the *np* and *lp* forms.

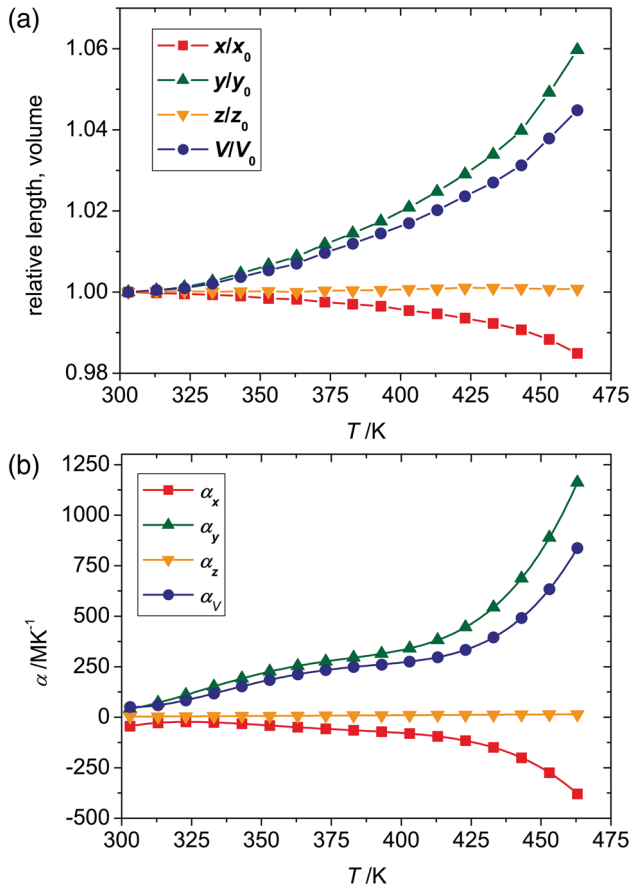

Figure 4. a) Relative expansion of the *np* form of **1** in the range from 303 to 463 K. The expansion of *x*, *y*, *z*, and *V* is shown in relation to the initial values at 303 K. b) Temperature dependent thermal expansion coefficients (α) for *x*, *y*, *z*, and *V* between 303 to 463 K. These data are based on empirical fits of the corresponding structural parameters of the heating branch of the VT-PXRD experiment.

compared to the very large hysteresis observed for MIL-53(Al) (≈200 K).[14b]

In detail, the thermal expansion of the *np* form of **1** in the range from 303 to 463 K is highly anisotropic (**Figure 4**). Vector *x* is showing NTE of –1.5% and *y* shows PTE of +6.0%, while *z* is almost constant. As a result the rhombic structural motif of the $[Zn_2(fu\text{-}L^1)_2]_n$ grids is continuously opening up with rising temperature whereas the distance between two adjacent $[Zn_2(fu\text{-}L^1)_2]_n$ grids (described by *z*) is nearly unaffected. The coefficients of thermal expansion (α) along *x*, *y*, and *z* as well as the volumetric thermal expansion coefficient α_V have been calculated from empirical fits in the range from 303 to 463 K (Figure 4b, see Supporting Information for details). At 303 K the NTE along *x* (α_x = –44 MK^{-1}) and PTE along *y* (α_x = +42 MK^{-1}) are in the moderate region. Both coefficients increase rapidly with the temperature, leading to extraordinary large expansivities at 463 K (α_x = –380 MK^{-1}, α_y = +1161 MK^{-1}). The volumetric coefficient of thermal expansion α_V is +51 MK^{-1} at 303 K and reaches +837 MK^{-1} at 463 K. These values are much higher than the 'colossal' thermal expansion coefficients of current record holders within the family of coordination networks and MOFs (α_a ≈ +230 MK^{-1}, α_c ≈ –170 MK^{-1}, α_V ≈ +300 MK^{-1} for FMOF-1;[18] α_a ≈ +150 MK^{-1}, α_c ≈ –130 MK^{-1}, α_V ≈ +170 MK^{-1} for $Ag_3[Co(CN)_6]$[15a]) and represent, to the best of our knowledge, the largest intrinsic expansivities reported for any crystalline material so far.[19] Remarkably, the magnitude of the volumetric thermal expansion coefficient of **1** is more comparable to the thermal expansion coefficients of liquid water (Supporting Information Figure S51), rather than crystalline solid-state materials.

At a threshold temperature (T_{th}) of 473 K the expansivity of **1** is so large, that phase transformation from the monoclinic *np* form to the tetragonal *lp* form occurs. This leads to coexistence of both phases, *np* and *lp*, between 473 to 483 K. Thereby, the fraction of *np* rapidly decreases while the fraction of *lp* increases (Supporting Information Figure S11). The transition is completed at 493 K and **1** exists solely as *lp* form, with *x* and *y* being equal. Hence, the *lp* form represents the most expanded structure possible for this material. Note, that

N,N-dimethylformamide or carbon dioxide loaded *lp* samples of **1** still feature a rhomb shaped motif ($x \neq y$) with a slightly lower specific volume. This important difference is assigned to packing and interaction effects of the guests with **fu** inside the pores.[10b,10c]

The phenomenon of thermal expansion in materials is commonly ascribed to the anharmonicity of their interatomic and intermolecular vibrational modes. Unusually large PTE and NTE in framework materials are often explained by transverse atomic or molecular displacements involving geometric flexing around 'hinges' of the crystalline structure.[15a–c,16,20] Similarly, the unique temperature dependent response of **1** is also based on a lattice fence-like hinged motion. However, the abnormally large expansivities of **1** just arise from the unique interplay between the structurally well defined framework backbone and the flexible disordered substituents (**fu**), which possess many degrees of freedom for rotations and vibrations in the (nano) confined pore space. In principle, the substituents can conceptually be viewed as *immobilized* guests, which are fixed at the much more rigid backbone. We propose that thermally excited vibrations of **fu**, which are coupled to the framework via L, are causing the massive expansion of *np* in the range from 303 to 463 K. At T_{th} the thermal energy is large enough to overcome the attractive intra-framework interactions allowing the framework to switch to *lp*, which provides more pore space for thermal motions of **fu**. Given that the thermal motion of the disordered side chains can hardly be quantified using diffraction techniques we have currently started investigating these effects with solid state VT-NMR spectroscopy of selectively deuterated $[Zn_2(fu\text{-}L)_2dabco]_n$ samples.

Similar studies on the related $[Zn_2(fu\text{-}L^k)_2dabco]_n$ (**2-4**, k = 2-4) frameworks indicate the drastic influence of the choice of **fu** on the thermo-responsive properties of these materials. At 298 K compound **2**, which features less polar *n*-butoxy substituents instead of the more polar 2-methoxyethoxy substituents of **1**, represents a *np* form very similar to **1** but with a slightly larger unit cell volume (Supporting Information Figure S2).[10c] Notice, that at the beginning of the VT-PXRD experiment a reflection of low intensity is apparent at $2\theta = 8.11°$, which is dedicated to a small fraction of **2** already featuring the *lp* form. Nevertheless, the vast majority of **2** exhibits the *np* form at 303 K, evidenced by the very low intensity of the aforementioned reflection. Le Bail fitting[17] of the VT-PXRD patterns of **2** (**Figure 5**) indicates, that the overall thermal behavior of **2** is related to the behavior of **1**. Vector *x* is contracting (NTE), *y* is expanding (PTE), and *z* is again almost invariable in the range from 303 to 393 K (**Figures 6** and **7**). The thermal expansion coefficients of **2** are already very large at 303 K ($\alpha_x = -74$ MK^{-1}, $\alpha_y = +283$ MK^{-1}, $\alpha_V = +209$ MK^{-1}) and, similar to **1**, increase further with the temperature ($\alpha_x = -186$ MK^{-1}, $\alpha_y = +674$ MK^{-1}, $\alpha_V = +524$ MK^{-1} at 393 K). As a consequence the *np*→*lp* transition starts at a threshold temperature of only 393 K and is already completed at 423 K. The much lower T_{th} of **2** is assigned to the weaker intermolecular interactions of the *n*-butoxy chains compared to the polar 2-methoxyethoxy chains present in **1**. Moreover, the phase transition shows an interesting hysteresis. Compound **2** remains exclusively in the *lp* form upon cooling from 473 K to a temperature as low as 363 K. Only below 353 K the reverse *lp*→*np* transition starts, leading to coexistence of

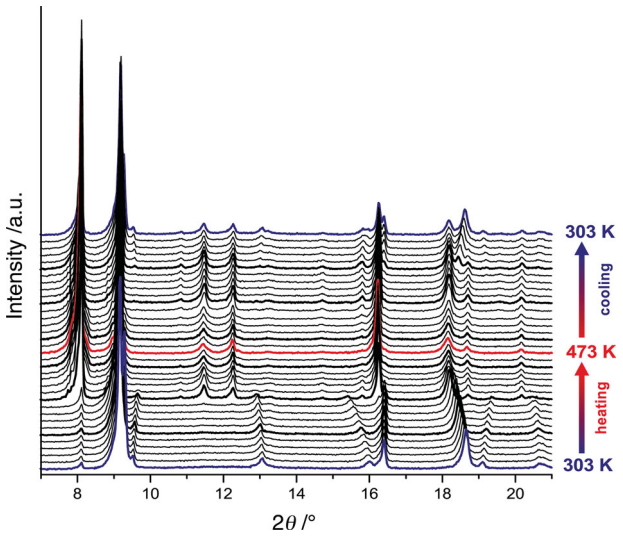

Figure 5. VT-PXRD patterns of $[Zn_2(fu\text{-}L^2)_2dabco]_n$ (**2**) recorded from 303 to 473 K (ΔT/step = 10 K).

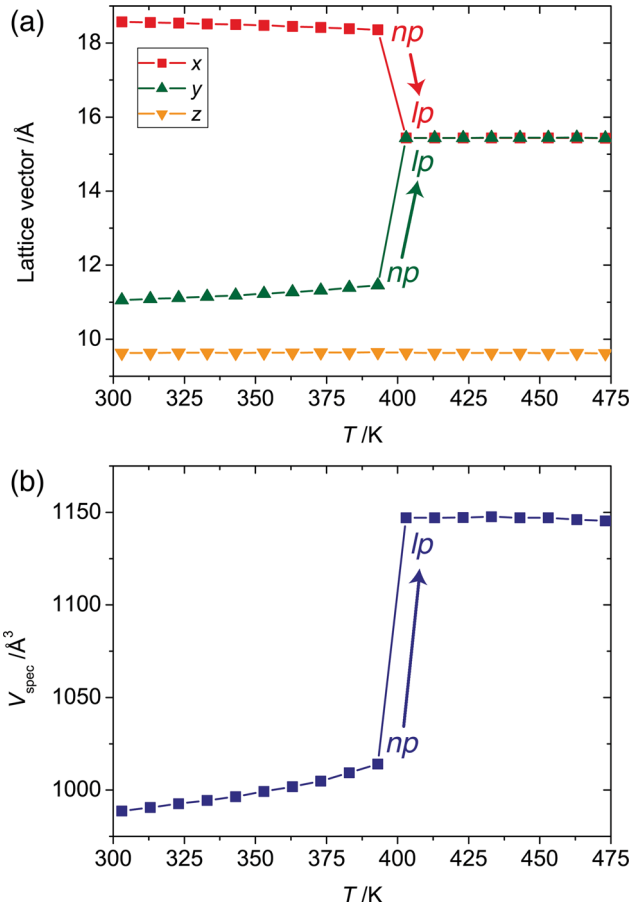

Figure 6. Temperature dependence of a) the characteristic lattice vectors *x*, *y*, *z* and b) V_{spec} of compound **2**. Data are based on the heating branch of the VT-PXRD experiment. The errors are not larger than the size of the symbols. At 403 and 413 K the contracted *np* form is also present as a minority phase, which is not included in the graphs.

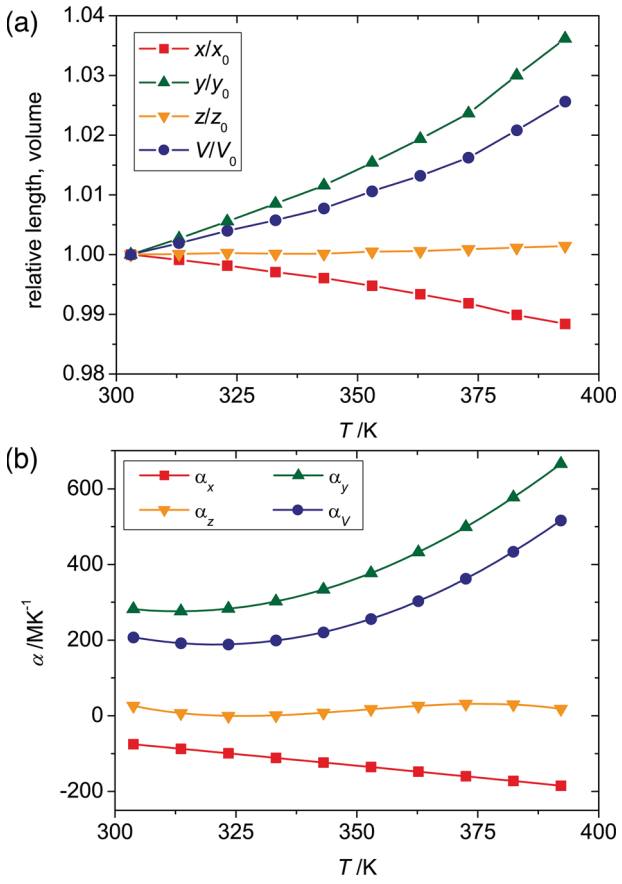

Figure 7. a) Relative expansion of the *np* form of **2** in the range from 303 to 393 K. The expansion of *x*, *y*, *z*, and *V* is shown in relation to the initial values at 303 K. b) Temperature dependent thermal expansion coefficients (α) for *x*, *y*, *z*, and *V* between 303 to 393 K. These data are based on empirical fits of the corresponding structural parameters of the heating branch of the VT-PXRD experiment.

both phases (Supporting Information Figure S15). The fraction of the *lp* form decreases and the fraction of the *np* form increases with falling temperature. At the final temperature of 303 K, however, both phases are still present and even after 13 days at 298 K the *lp*→*np* transition is not yet completed (Supporting Information Figure S16). The large hysteresis and very slow transformation of **2** upon cooling suggests that the *lp*→*np* transition is kinetically hindered for this material.

As expected, the related fu-MOFs **3** and **4**, which feature shorter ethoxy and *n*-propoxy substituents, do also show anisotropic thermal expansion upon heating to temperatures up to 513 K, but they do not transform to the *lp* form (Supporting Information Figure S17). Consequently, the chain length of the substituents has a major impact on the thermo-responsive behavior. Only $[Zn_2(fu\text{-}L)_2(dabco)]_n$ frameworks exhibiting linear substituents of five non-hydrogen atoms can be switched between the *np* and *lp* forms by means of temperature stimulus. If the chain is longer (six non-hydrogen atoms; e.g., *n*-pentoxy chain or 3-methoxypropoxy chain) the material is permanently in the *lp* form, irrespective of the presence of guests.[10a,10c]

Based on these results we synthesized and characterized binary mixed linker fu-MOFs of the type $[Zn_2(fu\text{-}L^1)_{2\text{-}2j}(fu\text{-}L^2)_{2j}$dabco$]_n$, $\mathbf{1}_{1\text{-}j}\mathbf{2}_j$ (j = 0.25, 0.50, 0.75). Mixed linker MOFs feature two or more topologically equivalent but differently functionalized linkers (here fu-L^1 *and* fu-L^2) as a solid solution inside one single-phased homogeneous framework.[21] Thereby, the linkers can be mixed in free ratios to adjust the properties of the framework beyond the limitations of the simple parent compounds.[10c,21a,21b] Le Bail fitting analysis[17] of PXRD patterns of compounds $\mathbf{1}_{1\text{-}j}\mathbf{2}_j$ recorded at 298 K prove that the obtained compounds are indeed single-phased (Supporting Information Figure S3–S5). VT-PXRD studies performed on $\mathbf{1}_{1\text{-}j}\mathbf{2}_j$ demonstrate that these mixed linker fu-MOFs feature thermo-responsive properties analogous to their parent frameworks **1** and **2** (Supporting Information Figure S18–S24). Importantly, the threshold temperature T_{th} for the *np*→*lp* transition, as well as the width of the hysteresis, are highly dependent on the applied molar ratio of fu-L^1 and fu-L^2.

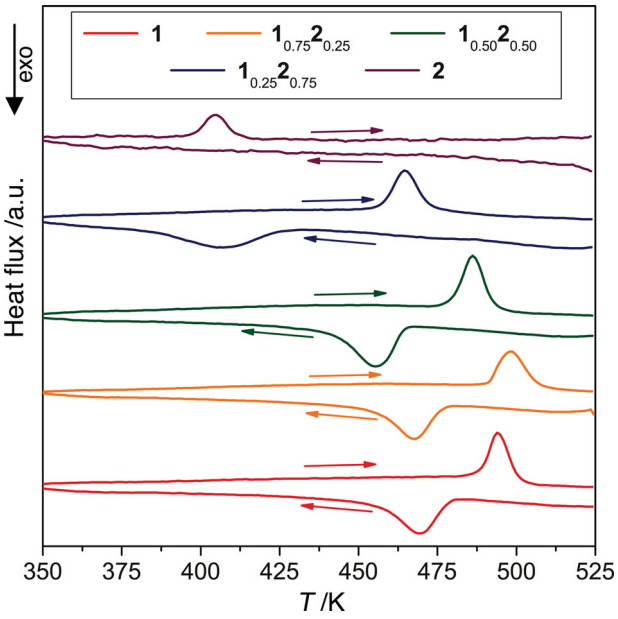

Figure 8. DSC curves of the simple fu-MOFs **1** and **2** in comparison to the curves of the mixed linker materials $\mathbf{1}_{1\text{-}j}\mathbf{2}_j$ (j = 0.25, 0.50, 0.75). Only the range from 350 K to 525 K is shown. Three consecutive cycles have been recorded of which only the second cycle is shown here (see the Supporting Information for details). The curves of the heating branch have been baseline corrected for the sake of clarity.

This is nicely illustrated by a comparison of DSC data recorded for $\mathbf{1}_{1\text{-}j}\mathbf{2}_j$ (j = 0.25, 0.50, 0.75) and the parent frameworks **1** and **2** (**Figure 8**). The *np*→*lp* transition generates an endothermic peak on the heating branch, while the reverse *lp*→*np* transition is apparent as an exothermic peak on the cooling branch. Three consecutive cycles in the temperature range from 303 to 523 K have been recorded in order to verify the reversibility of the phase transition (see Supporting Information). Notably, for the materials **1**, $\mathbf{1}_{0.75}\mathbf{2}_{0.25}$, and $\mathbf{1}_{0.50}\mathbf{2}_{0.50}$ the first runs yield slightly higher *np*→*lp* transition temperatures ($T_{np\rightarrow lp}$) compared to the second and third cycles (Supporting Information Figure S45, Table S5). However, no further changes are observed in the successive third runs. For that reason only the data derived from the second DSC cycles will be discussed here.

Table 1. Comparison of the phase transition temperatures and the corresponding phase transition enthalpies (ΔH) obtained from the DSC measurements. The data have been taken from the second cycle (see main text for details). Note, that there is no peak for the *lp*→*np* transition for **2**. As a result the calculated $\Delta H_{np\rightarrow lp}$ is considerably lower on the second cycle when compared to the first.

Sample	$T_{np\rightarrow lp}$ [K]	$\Delta H_{np\rightarrow lp}$ [kJ mol^{-1}]	$T_{lp\rightarrow np}$ [K]	$\Delta H_{lp\rightarrow np}$ [kJ mol^{-1}]
1	489	14.2	477	−15.3
$\mathbf{1}_{0.75}\mathbf{2}_{0.25}$	492	12.6	476	−14.9
$\mathbf{1}_{0.50}\mathbf{2}_{0.50}$	480	17.1	464	−19.1
$\mathbf{1}_{0.25}\mathbf{2}_{0.75}$	458	15.1	424	−16.9
2	398[a] (398)[b]	6.5[a] (13.1)[b]	–	–

[a]second cycle; [b]first cycle.

Unexpectedly, $T_{np\rightarrow lp}$ is slightly higher for $\mathbf{1}_{0.75}\mathbf{2}_{0.25}$ (491 K) when compared to pure **1** (489 K) giving rise to a nonlinear behavior of the thermo-mechanical properties on the linker ratio (**Table 1**). A further enrichment of fu-L^2 leads to the expected decrease of $T_{np\rightarrow lp}$ from 480 K for $\mathbf{1}_{0.50}\mathbf{2}_{0.50}$ to 458 K for $\mathbf{1}_{0.25}\mathbf{2}_{0.75}$. Compound **2** features a $T_{np\rightarrow lp}$ of only 398 K. These results are in very good agreement with the VT-PXRD data. Slight differences in the phase transition temperatures determined from VT-PXRD compared to the DSC data might originate from the comparatively fast heating/cooling rate of ±5 K min^{-1} used for the DSC measurements, while the samples have equilibrated for 10 min at the corresponding temperature before the VT-PXRD patterns have been recorded.

The reverse exothermic *lp*→*np* transition, which is taking place on the consecutive cooling branch of the DSC experiment, is at a similar temperature for **1** (477 K) and $\mathbf{1}_{0.75}\mathbf{2}_{0.25}$ (476 K). Increasing amounts of fu-L^2 decrease the *lp*→*np* phase transition temperature further to 464 K ($\mathbf{1}_{0.50}\mathbf{2}_{0.50}$) and 424 K ($\mathbf{1}_{0.25}\mathbf{2}_{0.75}$). As a result the temperature difference ΔT ($\Delta T = T_{np\rightarrow lp} - T_{lp\rightarrow np}$) between the related phase transitions is nonlinearly increasing with increasing amounts of fu-L^2 (ΔT = 12 K for **1**, ΔT = 15 K for $\mathbf{1}_{0.75}\mathbf{2}_{0.25}$, ΔT = 16 K for $\mathbf{1}_{0.50}\mathbf{2}_{0.50}$, and ΔT = 34 K for $\mathbf{1}_{0.25}\mathbf{2}_{0.75}$). Notice, on the cooling branch of the DSC experiment of **2** no exothermic peak, and therefore no phase transition is detected. This observation is in accordance with the VT-PXRD study on **2**, which shows a very slow transformation from the *lp* to the *np* form upon cooling. A significant fraction of **2** stays in the *lp* form, which is further evidenced by the strong decrease in phase transition enthalpy ΔH for the *np*→*lp* transition (Table 1 and S5) from 13.1 kJ mol^{-1} in the first cycle to only 6.5 kJ mol^{-1} in the second cycle. Such behavior is not seen for the other compounds, where ΔH is very similar in all cycles proving the complete reversibility of the thermal breathing of these fu-MOFs.

3. Conclusions

In summary we have demonstrated how extreme thermo-mechanical properties, including massive framework expansion comprising uniaxial NTE and PTE, as well as temperature responsive breathing, can be implemented in MOFs via the utilization of functionalized linkers featuring pendent flexible substituents. It is suggested that the unique thermo-mechanical behavior originates from increased thermal motions (vibrations, rotations) of the linear side chains with rising temperature. The interplay of the flexible substituents with the robust and structurally well-defined framework backbone leads to a remarkable structural response of these hybrid solid/liquid materials in dependence on the temperature. Importantly, chain length and chemical nature of the pendent side chains govern the particular properties of the respective MOF, which allows for a precise fine-tuning of the thermo-mechanical properties, according to the concept of mixed linker MOFs. In principle our novel methodology using (mixed) fu-Ls is transferable to a wide variety of other MOF systems and may facilitate the development of new functional hybrid materials for applications in sensing,[13] heat storage/transfer,[12c] or for temperature switchable devices.[22]

4. Experimental Section

Synthesis: The linkers and MOFs have been prepared and activated in vacuo as described elsewhere.[10a,10c] The evacuated (guest-free) samples have been stored in a glovebox under Ar atmosphere prior to analysis.

Powder X-Ray Diffraction: Room temperature powder X-ray diffraction (PXRD) patterns of the guest-free fu-MOFs have been recorded at 298 K on a Bruker D8 Advance AXS diffractometer with Cu Kα radiation and a Göbel mirror in θ-2θ geometry with a position-sensitive detector in a 2θ range from 5°–60° or 5°–50° at a scan speed of 1° min^{-1}. α-Al_2O_3 was employed as external standard. The samples have been filled into glass capillaries (ø = 0.7 mm) in a glovebox. Each capillary was subsequently sealed. Variable temperature powder X-ray diffraction (VT-PXRD) experiments were performed on a PANalytical X'PertPro with Cu Kα radiation in Bragg-Brentano geometry with an automatic divergence slit and a position sensitive detector using a continuous scan mode in the range of 2θ = 7°–20° or 6°–21°. A sample stage with a temperature controller and a heating plate (T = 303–1273 K) was utilized. The activated, ground MOF samples were deposited on a single crystalline silicon wafer, which was placed on the sample stage and accordingly capped with a graphite dome to generate a closed system. The VT-PXRDs have been recorded with a step size of 10 K and an equilibration time of 10 min before starting a data collection after the corresponding temperature was reached. Le Bail fitting analysis of the PXRD patterns was performed with RIETICA.[23]

Differential Scanning Calorimetry: Differential scanning calorimetry (DSC) was performed on a Netzsch STA 409 PC with a heating/cooling rate of ±5 K min^{-1} in a temperature range from 303 to 523 K. Three adjacent cycles were performed with each sample. The samples (mass = 10–40 mg) were placed in an alumina crucible inside a glovebox (Ar atmosphere). Data analysis was performed with the Netzsch Proteus Thermal Analysis software package. The phase transition temperatures have been determined from the peak onsets. The respective phase transition enthalpies ΔH_{trans} were obtained via integration of the DSC curves.

Supporting Information

Supporting Information is available from the Wiley Online Library or from the author.

Acknowledgements

S.H. gratefully thanks A. K. Cheetham for his support and the European Research Council for funding. S.H. acknowledges the Fonds der Chemischen Industrie (https://www.vci.de/fonds) and the

Ruhr-University Research School (http://www.research-school.rub.de) and A.S. acknowledges the Research Cluster SusChemSys (http://www.cmt.rwth-aachen.de/projects.html) for doctoral fellowships. The work was supported by the Priority Program 1362 "Metal-Organic Frameworks" (http://www.metal-organic-frameworks.de) and by the Cluster of Excellence RESOLV (EXC 1069; http://www.ruhr-uni-bochum.de/solvation) funded by the Deutsche Forschungsgemeinschaft.

Received: April 13, 2013
Published online: July 1, 2013

[1] See the Hybrid Materials themed issue of *Chem. Soc. Rev.* **2011**, *40*.
[2] a) S. Kitagawa, R. Kitaura, S.-I. Noro, *Angew. Chem. Int. Ed.* **2004**, *43*, 2334–2375; b) G. Ferey, *Chem. Soc. Rev.* **2008**, *37*, 191–214; c) U. Mueller, M. Schubert, F. Teich, H. Puetter, K. Schierle-Arndt, J. Pastré, *J. Mater. Chem.* **2006**, *16*, 626–636; d) J. L. C. Rowsell, O. M. Yaghi, *Microporous Mesoporous Mater.* **2004**, *73*, 3–14; e) B. Chen, S. Xiang, G. Qian, *Acc. Chem. Res.* **2010**, *43*, 1115–1124.
[3] L. J. Murray, M. Dincă, J. R. Long, *Chem. Soc. Rev.* **2009**, *38*, 1294–1314.
[4] J. R. Li, J. Sculley, H. C. Zhou, *Chem. Rev.* **2012**, *112*, 869–932.
[5] J. Lee, O. K. Farha, J. Roberts, K. A. Scheidt, S. T. Nguyen, J. T. Hupp, *Chem. Soc. Rev.* **2009**, *38*, 1450-1459.
[6] a) N. Rosi, D. Vodak, J. Wachter, M. O'Keeffe, O. Yaghi, *Science* **2002**; b) S. Biswas, T. Ahnfeldt, N. Stock, *Inorg. Chem.* **2011**, *50*, 9518–9526; c) D. Himsl, D. Wallacher, M. Hartmann, *Angew. Chem. Int. Ed.* **2009**, *48*, 4639–4642.
[7] S. M. Cohen, *Chem. Rev.* **2012**, *112*, 970–1000.
[8] a) H. Deng, M. A. Olson, J. F. Stoddart, O. M. Yaghi, *Nat. Chem.* **2010**, *2*, 439–443; b) Q. Li, W. Zhang, O. S. Miljanić, C.-H. Sue, Y.-L. Zhao, L. Liu, C. B. Knobler, J. F. Stoddart, O. M. Yaghi, *Science* **2009**, *325*, 855–859.
[9] S. Henke, A. Schneemann, S. Kapoor, R. Winter, R. A. Fischer, *J. Mater. Chem.* **2012**, *22*, 909–918.
[10] a) S. Henke, R. Schmid, J.-D. Grunwaldt, R. A. Fischer, *Chem. Eur. J.* **2010**, *16*, 14296–14306; b) S. Henke, D. C. Florian Wieland, M. Meilikhov, M. Paulus, C. Sternemann, K. Yusenko, R. A. Fischer, *CrystEngComm* **2011**, *13*, 6399–6404; c) S. Henke, A. Schneemann, A. Wütscher, R. A. Fischer, *J. Am. Chem. Soc.* **2012**, *134*, 9464–9474.
[11] D. N. Dybtsev, H. Chun, K. Kim, *Angew. Chem. Int. Ed.* **2004**, *43*, 5033–5036.
[12] a) S. Bureekaew, S. Shimomura, S. Kitagawa, *Sci. Technol. Adv. Mater.* **2008**, *9*, 014108; b) G. Férey, C. Serre, *Chem. Soc. Rev.* **2009**, *38*, 1380–1399; c) S. Horike, S. Shimomura, S. Kitagawa, *Nat. Chem.* **2009**, *1*, 695–704; d) B. Chen, C. Liang, J. Yang, D. S. Contreras, Y. L. Clancy, E. B. Lobkovsky, O. M. Yaghi, S. Dai, *Angew. Chem. Int. Ed.* **2006**, *45*, 1390–1393.
[13] L. E. Kreno, K. Leong, O. K. Farha, M. Allendorf, R. P. Van Duyne, J. T. Hupp, *Chem. Rev.* **2012**, *112*, 1105–1125.
[14] a) A. Ghoufi, A. Subercaze, Q. Ma, P. G. Yot, Y. Ke, I. Puente-Orench, T. Devic, V. Guillerm, C. Zhong, C. Serre, G. Férey, G. Maurin, *J. Phys. Chem. C* **2012**, *116*, 13289–13295; b) Y. Liu, J.-H. Her, A. Dailly, A. J. Ramirez-Cuesta, D. A. Neumann, C. M. Brown, *J. Am. Chem. Soc.* **2008**, *130*, 11813–11818; c) M. Mendt, B. Jee, N. Stock, T. Ahnfeldt, M. Hartmann, D. Himsl, A. Pöppl, *J. Phys. Chem. C* **2010**, *114*, 19443–19451; d) P. G. Yot, Q. Ma, J. Haines, Q. Yang, A. Ghoufi, T. Devic, C. Serre, V. Dmitriev, G. Férey, C. Zhong, G. Maurin, *Chem. Sci.* **2012**, *3*, 1100; e) A. M. Walker, B. Civalleri, B. Slater, C. Mellot-Draznieks, F. Cora, C. M. Zicovich-Wilson, G. Roman-Perez, J. M. Soler, J. D. Gale, *Angew. Chem. Int. Ed.* **2010**, *49*, 7501–7503.
[15] a) A. L. Goodwin, M. Calleja, M. J. Conterio, M. T. Dove, J. S. Evans, D. A. Keen, L. Peters, M. G. Tucker, *Science* **2008**, *319*, 794–797; b) M. Calleja, A. L. Goodwin, M. T. Dove, *J. Phys.: Condens. Matter* **2008**, *20*, 255226; c) J. L. Korcok, M. J. Katz, D. B. Leznoff, *J. Am. Chem. Soc.* **2009**, *131*, 4866–4871; d) Y.-S. Wei, K.-J. Chen, P.-Q. Liao, B.-Y. Zhu, R.-B. Lin, H.-L. Zhou, B.-Y. Wang, W. Xue, J.-P. Zhang, X.-M. Chen, *Chem. Sci.* **2013**, *4*, 1539–1546.
[16] a) D. Dubbeldam, K. S. Walton, D. E. Ellis, R. Q. Snurr, *Angew. Chem. Int. Ed.* **2007**, *46*, 4496–4499; b) J. M. Ogborn, I. E. Collings, S. A. Moggach, A. L. Thompson, A. L. Goodwin, *Chem. Sci.* **2012**, *3*, 3011–3017; c) L. D. DeVries, P. M. Barron, E. P. Hurley, C. Hu, W. Choe, *J. Am. Chem. Soc.* **2011**, *133*, 14848–14851; d) S. S. Han, W. A. Goddard, *J. Phys. Chem. C* **2007**, *111*, 15185–15191; e) N. Lock, Y. Wu, M. Christensen, L. J. Cameron, V. K. Peterson, A. J. Bridgeman, C. J. Kepert, B. B. Iversen, *J. Phys. Chem. C* **2010**, *114*, 16181–16186; f) I. Grobler, V. J. Smith, P. M. Bhatt, S. A. Herbert, L. J. Barbour, *J. Am. Chem. Soc.* **2013**, *135*, 6411–6414.
[17] A. Le Bail, H. Duroy, J. L. Fourquet, *Mater. Res. Bull.* **1988**, *23*, 447–452.
[18] C. Yang, X. Wang, M. A. Omary, *Angew. Chem. Int. Ed.* **2009**, *48*, 2500–2505.
[19] Recently, a porous Ni-MOF was reported to exhibit a uniaxial PTE coefficient of upto 430 MK^{-1} (ref. 15d). However, the large PTE is only observed for the *N*,*N*-dimethylformamide and the methanol loaded MOF. The guest-free framework exhibits a significantly smaller uniaxial thermal expansion coefficient of 81 MK^{-1}. Hence the large thermal expansion of the solvated framework can mainly be ascribed to the adsorbed guests and is not an intrinsic framework property.
[20] A. D. Fortes, E. Suard, K. S. Knight, *Science* **2011**, *331*, 742–746.
[21] a) T. Fukushima, S. Horike, Y. Inubushi, K. Nakagawa, Y. Kubota, M. Takata, S. Kitagawa, *Angew. Chem. Int. Ed.* **2010**, *49*, 4820–4824; b) H. Deng, C. J. Doonan, H. Furukawa, R. B. Ferreira, J. Towne, C. B. Knobler, B. Wang, O. M. Yaghi, *Science* **2010**, *327*, 846–850; c) S. Marx, W. Kleist, J. Huang, M. Maciejewski, A. Baiker, *Dalton Trans.* **2010**, *39*, 3795–3798; d) W. Kleist, F. Jutz, M. Maciejewski, A. Baiker, *Eur. J. Inorg. Chem.* **2009**, 3552–3561; e) W. Kleist, M. Maciejewski, A. Baiker, *Thermochimica Acta* **2010**, *499*, 71–78; f) T. Lescouet, E. Kockrick, G. Bergeret, M. Pera-Titus, S. Aguado, D. Farrusseng, *J. Mater. Chem.* **2012**, *22*, 10287; 21g) H. Chun, D. N. Dybtsev, H. Kim, K. Kim, *Chem. Eur. J.* **2005**, *11*, 3521–3529; h) A. D. Burrows, *CrystEngComm* **2011**, *13*, 3623–3642.
[22] a) M. A. Stuart, W. T. Huck, J. Genzer, M. Muller, C. Ober, M. Stamm, G. B. Sukhorukov, I. Szleifer, V. V. Tsukruk, M. Urban, F. Winnik, S. Zauscher, I. Luzinov, S. Minko, *Nat. Mater.* **2010**, *9*, 101–113; b) Y. Sakata, S. Furukawa, M. Kondo, K. Hirai, N. Horike, Y. Takashima, H. Uehara, N. Louvain, M. Meilikhov, T. Tsuruoka, S. Isoda, W. Kosaka, O. Sakata, S. Kitagawa, *Science* **2013**, *339*, 193–196.
[23] B. A. Hunter, C. J. Howard, *A computer program for Rietveld analysis of X-ray and neutron powder diffraction patterns*, Lucas Heights Laboratories, **1998**.